2020

A Novel Ground Fault Detection Method for Electric Vehicle Powertrains Based on a Grounding Resistor Voltage Analysis

J.M. GUERRERO, G. NAVARRO, C. A. PLATERO, P. TIAN AND F. BLÁZQUEZ

This is an “Accepted article” version of a paper and it is not the “Final published article” version as appearing in IEEE Transactions on Industrial Applications, Volume: 56, Issue: 4, September-October 2020).and published on 09 June 2020

How to Cite this article:

M. Guerrero, G. Navarro, C. A. Platero, P. Tian and F. Blázquez, "A Novel Ground Fault Detection Method for Electric Vehicle Powertrains Based on a Grounding Resistor Voltage Analysis," in *IEEE Transactions on Industry Applications*, vol. 56, no. 5, pp. 4934-4944, Sept.-Oct. 2020, doi: 10.1109/TIA.2020.3000965.

DOI: https://doi.org/10.1109/TIA.2020.3000965

A Novel Ground Fault Detection Method for Electric Vehicle Powertrains Based on a Grounding Resistor Voltage Analysis

J. M. Guerrero, G. Navarro, C. A. Platero, *Member, IEEE*, P. Tian and F. Blázquez, *Member, IEEE*.

***Abstract*—The growing adoption of electric vehicles has recently attracted increasing attention of scientists and brought about pioneering research studies from various fields. Safety concerns particularly those regarding ground faults detection and protection, have extensively been addressed. Ground faults occur quite frequently in electric vehicles and they may be due to severe operation conditions, such as vibrations, twists or even crashes. Generally, the first ground fault is not dangerous, since the powertrain systems, namely, the DC bus where the batteries are connected, the power inverter and one or more AC machines, are generally ungrounded. The second ground fault, however, can produce malfunction in some systems, power loss or even serious damages. Locating the fault has often proved hard and time-consuming. For this reason, the present study focuses on developing a ground-fault detection method for electric vehicles capable of determining on which side, the DC or the AC, the ground fault is located. The method is based on the analysis of the voltage in a grounding resistor connected between the midpoint of the battery pack and ground. Based on the polarity and harmonics, it is possible to locate the ground fault. This method has been verified excellent results have been achieved using computer simulations and experimental tests in a 140-kW electronic power inverter fed by a 480 Vdc battery.**

***Index Terms*—Electric vehicles, Electrical fault detection, Fault location, Fault diagnosis, Power system protection.**

I. Introduction

SINCE last century, development in technology has brought major changes to our world. Two of the most discernible impacts are the increasing level of pollution and global warming.

Conventional vehicles depend on fossil fuels producing greenhouse gasses causing negative effects in our planet. Nowadays, there is an increasing interest in replacing these ones by electric vehicles (EVs), as they induce an efficient decarbonization process. The EU and USA have made several legislative tests procedures to define the fuel economy with effective vehicle range classifications of alternatively powered transport methods.

To develop a competent EV, the control system characteristics and the battery capacity are problems that both must be addressed.

However, these improvements for the EVs have some obstacles due to their high price, which mainly depends on the battery's life cycle and capacity and which cause the lack of investments. For example, electrical faults in the DC or AC circuits might reduce the life of the equipment, decreasing the life expectancy of the EV. Therefore, numerous protection methods and devices have been developed. One of these methods was previously presented in [1].

It is normal practice in EV to use ungrounded DC and AC systems, which means that it is not connected to the chassis. Thus, the positive and negative poles are insulated from the ground as well as the AC circuit. When a ground fault takes place (for example because of isolation degradation, vibrations occasioned by poor conditions of the road, sharp turns or a crash [2]), and only one pole is grounded, there is no large fault currents. However, long-term operation with one ground fault is not recommended. The voltage stress in the healthy pole will increase and the possibility of having a second ground fault will increase as well. If the other pole is also grounded, a short circuit happens. It could cause the incorrect operation of the vehicle, the early death of the affected components or even fire [3].

The traction motors of EVs are normally an AC type. Therefore, there are some inverters to feed the motors. It is also possible to have ground faults in the AC side of the circuit because of the same factors expressed before, and also because of the deterioration of the traction motors, which are the components most exposed to adverse conditions [4].

The ground fault detection and location are highly active research fields. A great number of research studies have recently been carried out, for instance, in microgrids [5]-[6], in HVDC [7], in railways [8], in shipboard [9], or in photovoltaic power plants [10], among others. Also, other studies on EVs have focused on faults in power electronics components [11], or traction motors [12]-[13].

In the case of the electric powertrain system of an EV or other systems with this electrical topology, one of the challenges to detecting ground faults resides in knowing if the fault is in the DC side or in the AC side of powertrain, which

This work was supported in part by Universidad Politécnica de Madrid and part by the Centro de Investigaciones Energéticas, Medioambientales y Tecnológicas (CIEMAT) of Spain.

J.M. Guerrero, C.A. Platero, P. Tian and F. Blázquez are with the Automatic, Electric and Electronic and Industrial Computing Department, ETSII, Universidad Politécnica de Madrid, Madrid 28006 (Spain). E-mails: josemanuel.guerrero.granados@alumnos.upm.es, carlosantonio.platero@upm.es, p.tian@alumnos.upm.es and francisco.blazquez@upm.es.

G. Navarro is with the Spanish Public Research Centre on Energy, Environment and Technology, CIEMAT, Ministerio de Innovación, Ciencia y Universidades, Madrid 28037 (Spain). E-mail: gustavo.navarro@ciemat.es.

is the main problem for the majority of protection relays currently in force for the protection against ground faults [14].

This paper presents a new method for ground fault detection in the powertrains of electrical vehicles. This work was presented previously in [1], and now is proved with additional experimental results. This method is based on the installation of a grounding resistor between the midpoint of the battery and the ground. In case of a ground fault, the method is able to detect faults by measuring the voltage in the grounding resistor. Also, the method distinguishes where the fault is, according to the polarity of this voltage in case of a DC fault, or harmonics of the wave in case of an AC fault.

The paper is structured as follow: Section II presents a brief overview of the ground fault location methods in DC and AC systems. Then, Section III details the principles of the proposed ground fault location technique. Section IV describes the simulation model and analyzes the computer simulations results of the operation of the proposed approach and Section V shows the experimental results achieved in an electronic power inverter. Finally, Section VI concludes with the main contributions of the paper.

II. State of the Art

There are numerous techniques for the detection of ground faults in DC systems. These detection techniques generally require a ground connection and the use of an external AC or DC voltage source or a low-frequency signal-injector [15]. These methods are based on the supervision of the current supplied by the external source and can be used in EVs.

As the electrical system is ungrounded, it is difficult to detect the first ground fault because of the low fault current values, especially in case of high resistance ground faults [16]. Moreover, most of the conventional diagnosis devices cannot locate the ground fault if it is in the DC side or AC side of the powertrain. An example of it can be a zero current injector in the DC side of the system [17].

An alternative way for current measurement is the differential monitoring in battery terminals and the detection of a potential leakage current [18].

Nowadays, some location and diagnosis systems designed for electric vehicles consist of two independent systems which measure and contrast the leakage current or the voltage waveform. Then, they determine if the fault is in the DC side or the AC side [19]-[20].

On the one hand, the diagnosis devices used to locate faults in DC systems are scarce. In this field, some prototype of Battery Management System, BMS, software functions have started using this type of systems, but they can only be used in DC circuits with batteries [21].

On the other hand, there are several techniques to detect ground faults in the AC systems. In case of AC insulated three-phase systems, one of the most employed method is based on the measurement of the residual voltage or the monitoring of the leakage current through the capacities to ground [22]. Under-impedance relays can be used as well to locate the problem in the AC side [23].

As previously explained, there are two different circuits in an EV, DC and AC connected by one or more frequency inverters. In case of a ground fault in any side of the electric powertrain, the fault current will be supplied by the battery.

The excitation systems of synchronous machines are similar to the EVs powertrains, where DC and AC circuits are mixed through inverters. In excitation systems, there are some research lines to distinguish faults in the DC or AC side of the excitation [24]. Moreover, there is also a technique to locate the fault in the field winding of the synchronous machine [25].

III. Operation Principles of the Novel Ground Fault Location Method

The proposed method is based on the connection of the midpoint of the battery pack to ground through a high value resistance (Grounding resistor, R_{gnd}). In case of a ground fault, the fault current will flow through the grounding resistor, and the high value of the grounding resistor limits the fault current, so the electrical operational conditions are not affected. The value of the grounding resistor should be chosen to satisfy the different electrical vehicles safety standards and regulations.

Then, the voltage on the grounding resistor will be measured. If the voltage is higher than a certain threshold a ground fault would be determined. Next, an analysis of the signal is done which allows to distinguish if the fault has taken place in the DC or AC side of the system.

Fig. 1 shows the layout of the ground fault location method. In this figure, a battery with a DC midpoint accessible and two AC traction motors fed by two inverters are shown.

In this system, during normal operation there is no current flowing through the grounding resistor, then, the voltage in R_{gnd} is null. However, in case of ground fault, a current through the grounding resistor appears and the voltage of the grounding resistor is measured and analyzed.

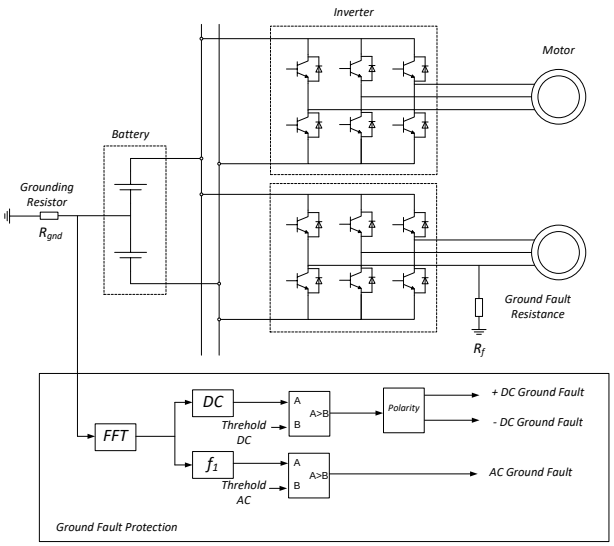

Fig. 1. Ground fault location lay out with a ground fault in the AC side with a ground fault resistance.

A. Ground fault in the DC side

Firstly, in the event of a ground fault on the DC side, the fault current will flow through the grounding resistor. In this case, the fault current is DC current. The value of the current is inversely proportional to the ground fault resistance, R_f.

The polarity of the grounding resistor voltage depends on the location of the ground fault. In case of a fault in the positive pole, the voltage polarity will be negative and in case of a fault in the negative pole the polarity will be positive.

B. *Ground fault in the AC side*

Secondly, in case of ground fault in the AC side, the fault current is alternating current.

Thanks to the FFT calculation of the grounding resistor voltage, the main frequency of the signal, which corresponds to the fundamental inverter frequency (f_1), can be determined. If it is a system with multiple inverters, knowing the operation frequencies of each inverter, one can determine which inverter is responsible for feeding the ground fault.

This method allows to identify DC or AC ground faults. The sensibility of the protection could be adjusted according to different fault resistances by setting the thresholds.

The peak value of the grounding resistor voltage (U_{gnd}) depends on the grounding resistor (R_{gnd}) , the ground fault resistance (R_f) and the batterie voltage (U). It can be expressed according to (1).

$$U_{gnd} = \frac{R_{gnd}}{R_f + R_{gnd}} \cdot \frac{U}{2} \quad (1)$$

IV. Computer Simulations

In order to validate the proposed method, numerous simulations have been performed for two different cases. The first case is a simulation using a squirrel cage motor fed by a inverter and in the second a passive RL is used as load.

A. *Simulation model with a squirrel cage motor.*

Fig. 2 shows the computer simulation model built in MATLAB Simulink ®. In this model, the grounding resistor, R_{gnd}, which is connected in the middle point of a 480 V battery can be observed.

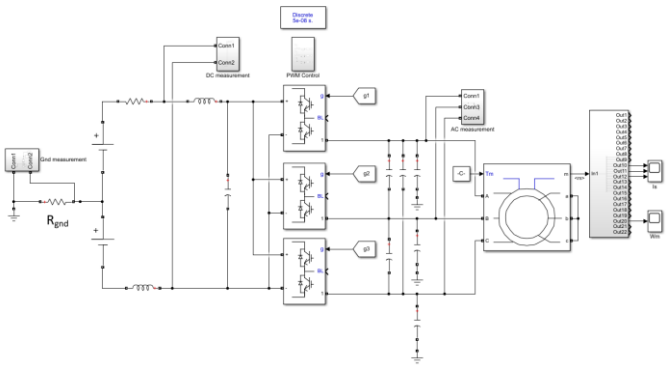

Fig. 2. Computer simulation model for a squirrel cage induction machine.

The battery pack is represented by two 240 V batteries connected in series and in parallel with them there is a capacitor of 1.638 mF. In the midpoint of the battery, a 4.7 kΩ grounding resistor is connected and its voltage waveform is displayed in an oscilloscope. Therefore, the maximum ground fault current is limited to 51 mA, although the system can operate with other grounding resistance values.

An inverter is connected to the DC bus bar to feed the induction machine. In case of having multiple batteries configuration, the midpoint of any parallel branch can be used for the grounding resistor connection, with identical results. This means that only a grounding resistor is needed and it does not matter where it is connected as long as it is in the midpoint of a branch.

As the ground fault current should be limited, the grounding resistor is set to 4.7 kΩ. In this case, the fault current is limited to 102 mA. For this configuration, the phase to ground voltage waveform in the AC side is shown in Fig. 3 as well as the current in Fig. 4.

Due to the similarity in the voltage and current waveforms with a passive RL dipole when the motor operates in nominal conditions, the simulations are done with an inductive charge.

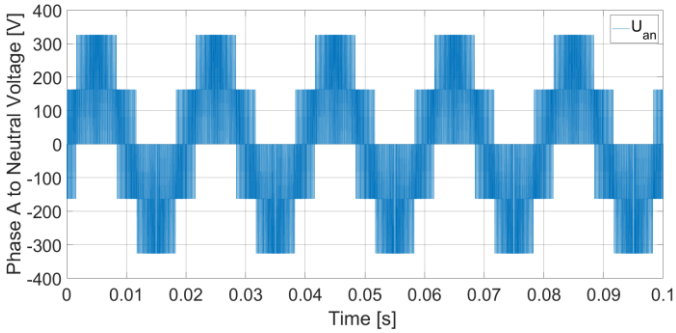

Fig. 3. Voltage phase to neutral in phase A measured from a simulation of the squirrel cage induction machine in healthy conditions.

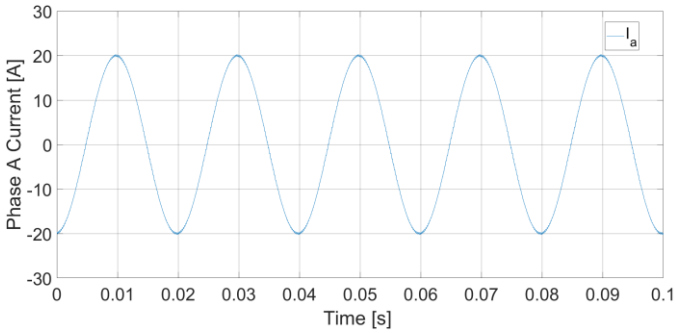

Fig. 4. Current of the induction machine in phase A measured from a simulation in healthy conditions.

B. *Simulation model with RL load*

The ground faults' simulations have been done with inductive loads connected in star with the neutral connection accessible as can be seen in Fig. 5.

In this circuit, the impedances taken into consideration have been 50 + jω0.0002 Ω per phase. The inductive part of the impedance represents the parasitic inductance. Also, mutual and phase to ground capacitive parasitic effects have been considered assuming values of 0.1 and 0.25 pF respectively as well as 0.3 mH inductive filters in series.

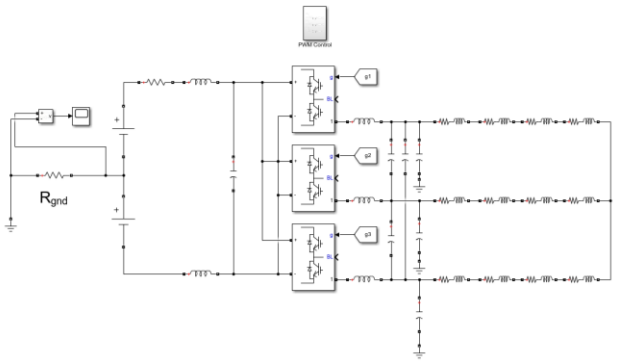

Fig. 5. Computer simulation model for RL load in the AC side of the inverter.

For this model, several simulations have been performed for ground fault resistance's (R_f) values of 0 Ω, 2.3 kΩ, 4.7 kΩ and 10 kΩ to verify the proper operation of the ground fault location system.

Furthermore, under healthy conditions, i.e., without any ground faults, the operation has been simulated, achieving AC waves similar to the squirrel cage simulations. These simulation results for RL load are shown in Fig. 6 and Fig. 7 where phase voltage and current are displayed respectively.

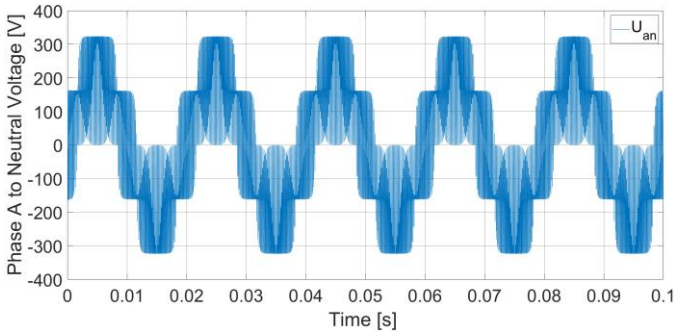

Fig. 6. Voltage phase to neutral in phase A measured from a simulation of the RL loads in healthy conditions.

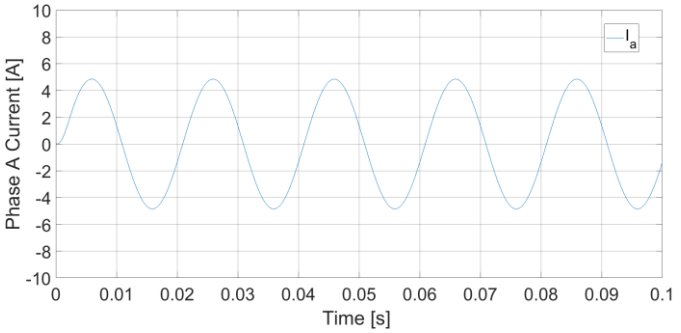

Fig. 7. Current in phase A measured from a simulation of the RL load in healthy conditions.

The results of the voltage measurement in the grounding resistor under healthy conditions are presented in Fig 8. It can be observed that the current through the grounding resistor is zero and consequently, so is the measured voltage. The high frequency disturbances in the grounding resistor measurement are provoked by the parasitic capacitances.

C. DC Side positive pole ground faults simulations

Next, the simulations with a ground fault in the positive terminal of the DC side were performed for the RL load scenery. In these simulations, the grounding resistor value remains at 4.7 kΩ. The fault resistances used are 0 Ω, 2.3 kΩ, 4.7 kΩ and 10 kΩ, respectively.

The results are shown in Fig. 8. It can be noticed that the voltage measurements for the simulation with the higher value of the ground resistance is the nearest value to the non-fault case. However, if the ground fault resistance is small or zero (Case 0 Ω), the voltage in the grounding resistor is close to half voltage of the battery. Also, the voltage measured could be affected by the ground fault location as can be seen in (1), where U/2 is the voltage between the ground fault location and the grounding resistor energized terminal. In this paper, only simulations at the location of 100% of the DC positive pole have been carried out, varying the ground fault arc resistances.

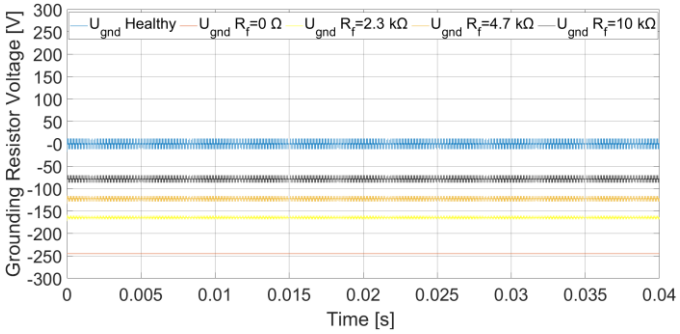

Fig. 8. Voltage waveform on the grounding resistor. Healthy state and ground faults in positive pole of the DC side. [Fault resistances 0 Ω, 2.3 kΩ, 4.7 kΩ and 10 kΩ].

D. DC side negative pole ground faults simulations

The next simulations set corresponds to ground faults in the negative pole of the DC side. The values of the grounding resistor and fault resistors are the same as in the previous simulations.

The results are presented in Fig. 9. These results are analogous to the previous cases, but the polarity of the voltage in the grounding resistor is positive.

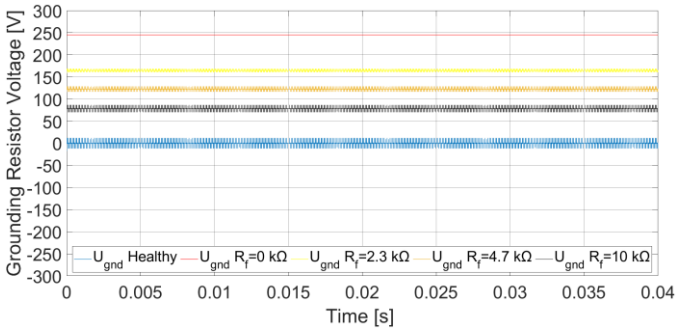

Fig. 9. Voltage waveform on the grounding resistor. Healthy state and ground faults in negative pole of the DC side. [Fault resistances 0.02Ω, 2.3kΩ, 4.7kΩ and 10 kΩ].

E. DC Side simultaneous positive and negative ground faults simulations.

Finally, the particular case of a double simultaneous ground fault in the positive and the negative terminals is studied in this subsection. In this case, three different sceneries are contemplated attending to the fault resistances values, R_{f+} and R_{f-} for the positive and the negative terminals, respectively.

The first one is a simultaneous symmetrical fault, where both fault resistances are identical. The proposed method cannot detect it, because the circuit is symmetrical, and no leakage current circulates through R_{gnd}. This fault should be detected by other device as an overcurrent relay. In Fig. 10, a simulation corresponding to this fault is carried out with 2.3 kΩ fault resistances in both terminals.

Another possibility is the asymmetrical double ground faults. In Fig. 10, two additional double fault simulations have been displayed. In both cases the fault resistances are 4.7 kΩ and 2.3 kΩ. The first one considers an imbalance with a higher fault resistance in the positive terminal (R_{f+} = 4.7 kΩ and R_{f-} = 2.3 kΩ). This means a higher leakage current becoming from

the negative pole due to its lower fault resistance, and consequently, the voltage measured in the grounding resistor will be positive. In the analogous case (R_{f+} = 2.3 kΩ and R_{f-} = 4.7 kΩ) the voltage will be negative due to the further weakening in the positive terminal.

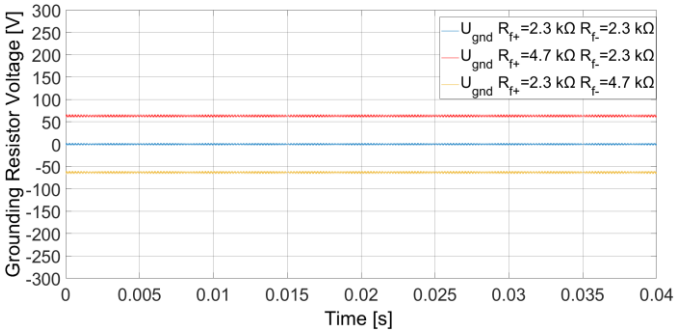

Fig. 10. Voltage waveform on the grounding resistor. A symmetrical ground fault in positive and negative pole and two asymmetrical faults [R_{f+} and R_{f-} 2.3 kΩ and 2.3 kΩ, 4.7 kΩ and 2.3 kΩ, and 2.3 kΩ and 4.7 kΩ respectively].

F. AC Side ground faults simulations

Furthermore, simulations with a ground fault in the AC side have been performed. When a ground fault takes place in the AC side, an alternating current flows through the grounding resistor. The amplitude of the voltage wave in the grounding resistor is inversely proportional to the fault resistance.

The results are shown in Fig. 11, Fig. 12 Fig. 13 and Fig. 14 for fault resistances of 0 Ω, 2.3 kΩ, 4.7 kΩ and 10 kΩ, respectively.

In these cases, instead of a direct voltage (as it appears in case of a DC faults), an alternating pulsed voltage wave is measured in the grounding resistance.

The sinusoidal oscillations are given by the parasitic inductances and capacitances and inductive filters.

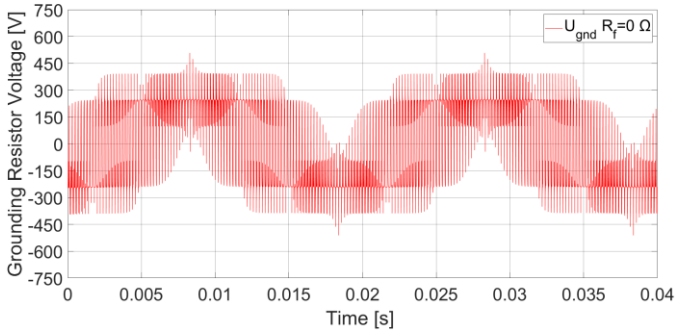

Fig. 11. Voltage waveform on the grounding resistor. Ground fault in the AC side. [Fault resistance 0 Ω].

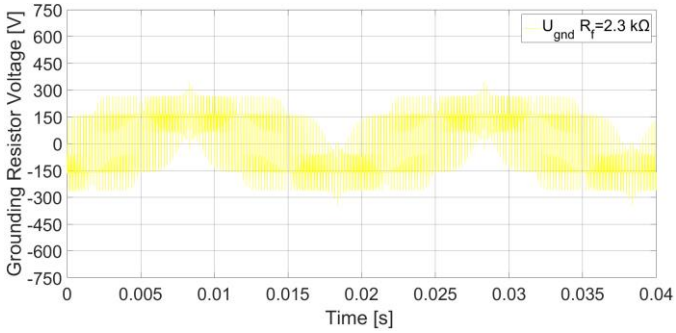

Fig. 12. Voltage waveform on the grounding resistor. Ground fault in the AC side. [Fault resistance 2.3 kΩ].

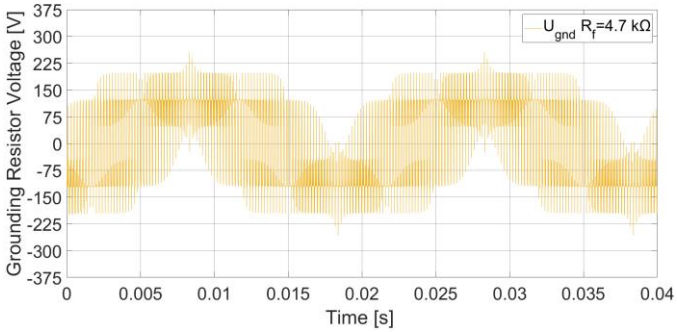

Fig. 13. Voltage waveform on the grounding resistor. Ground fault in the AC side. [Fault resistance 4.7 kΩ].

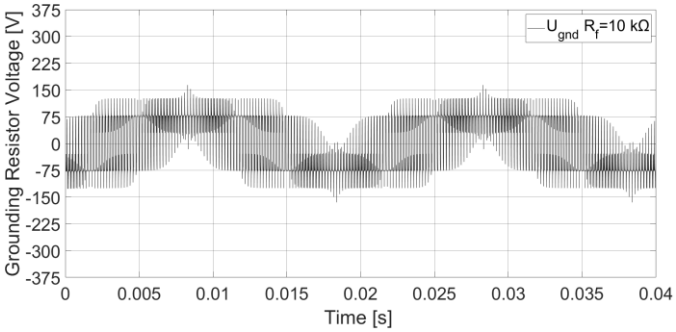

Fig. 14. Voltage waveform on the grounding resistor. Ground fault in the AC side. [Fault resistance 10 kΩ].

From Fig. 11, Fig. 12, Fig. 13 and Fig. 14 it can be clearly observed that the higher the value of fault resistance is, the smaller the AC voltage appears in the grounding resistor. It is because most of the difference of potential is assumed in the fault resistance, keeping few volts in the ground resistor, as has been expressed in (1).

In Table I the FFT analysis is presented corresponding to the fundamental inverter frequency (f_1=50Hz), the inverter commutation frequency (5 kHz) and the DC component.

As exposed before the DC faults have DC component, while the rest of harmonics are negligible. Analogously, in AC ground faults, the higher harmonics correspond to the fundamental frequency, f_1, and the commutation frequency.

TABLE I
GROUNDING RESISTOR VOLTAGE FFT SIMULATION RESULTS FOR DIFFERENT GROUND FAULTS

Type of fault and fault resistance, R_f	**$\|U_{DC}\|$ [V]**	**$\|U_{f1}\|$ [V]**	**$\|U_{5kHz}\|$ [V]**
DC Pole + ground fault			
R_f = 0	239.94	0.31	8.24×10^{-3}
R_f = 2.3 kΩ	161.11	0.23	2.98×10^{-4}
R_f = 4.7 kΩ	119.98	0.15	4.14×10^{-3}
R_f = 10 kΩ	76.72	0.11	2.64×10^{-3}
DC pole – ground fault			
R_f = 0	239.99	0.01	1.22×10^{-4}
R_f = 2.3 kΩ	164.49	0.01	6.86×10^{-5}
R_f = 4.7 kΩ	122.50	0.01	4.37×10^{-5}
R_f = 10 kΩ	78.33	0.00	2.22×10^{-5}
AC phase ground fault			
R_f = 0	2.48	242.66	145.65
R_f = 2.3 kΩ	1.66	162.86	97.81
R_f = 4.7 kΩ	1.24	121.28	72.84
R_f = 10 kΩ	0.79	77.55	46.58

V. Experimental Results

To bear out the method, numerous experiments have been carried out in a 140 kW power inverter. In this section, the experimental setup and experimental results are presented.

A. Experimental setup

The system consists of a 140 kW three-phase inverter fed with a 480 V battery composed from 40 modules in series. The inverter provides AC current to a 50 Ω three-phase resistor, composed by four 12.5 Ω resistors connected in series, which allows the connections between them to provoke ground faults.

Table II shows the ratings for each component of the experimental setup. Also, in Fig 15 the battery set is presented. The power electronic inverter is shown in Fig. 16 and its control hardware can be observed in Fig. 17. The control of the power inverter was done as a voltage source inverter (VSI), adjusting the duty to achieve 205 V_{RMS} phase to ground.

Finally, in Fig. 18 and Fig. 19 the resistive load, the grounding resistor and the measurement devices are illustrated. The fault was performed by commutating a switcher connected between the circuit and a fault resistance of 0 Ω, 2.3 kΩ, 4.7 kΩ and 10 kΩ to do the tests (Fig.20).

TABLE II
Experimental Setup Ratings

Component	Characteristic	Magnitude
Battery	U_{DC}	480 V
	U_{DC} per cell	12 V/cell
	Modules per String	40
	I_N	3.6 A
	Q	12 Ah
	Internal R	12 mΩ
Inverter	Power	140 kW
	U_{DC} max.	900 V
	I_{out} max.	200 A
	f max.	25 kHz
	C	1.638 mF
Resistor	R	12.5 Ω
	P	392 W
	Total Three-phase Power	4704 W

Fig. 15. Battery set for the experiments. 480 V in a string of 40 modules of 12 V per module.

Fig. 16. Power inverter.

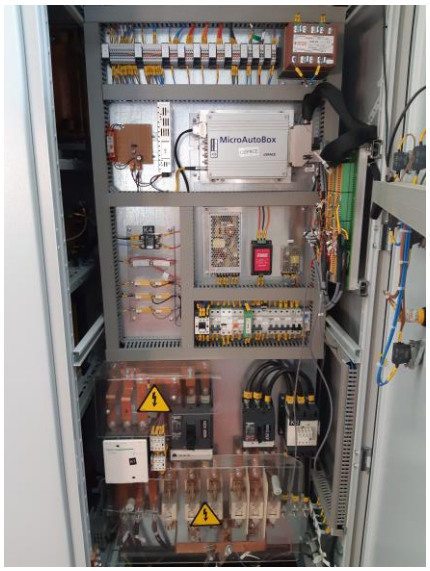

Fig. 17. Power inverter control unit, DSP, and protection systems.

Fig. 18. Three-phase resistive load in terminals of the power inverter.

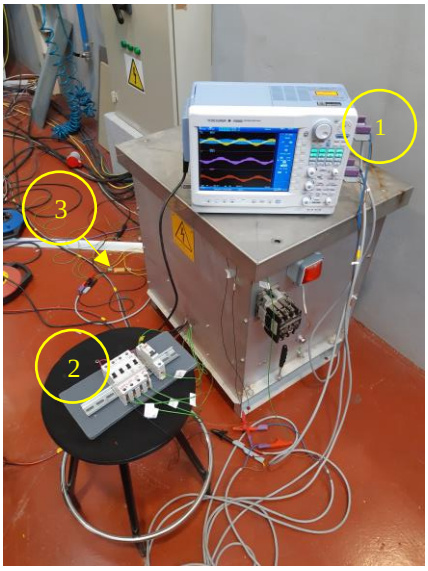

Fig. 19. Measurement devices (1), fault position changer (2), and the grounding resistor (3).

As in the simulations, a grounding resistor of 4.7 kΩ was connected to the midpoint of the battery to ground and some ground fault resistors were connected to the ground as well.

In Fig. 20, the electrical scheme of the installation is displayed. First, the batteries and the grounding resistor are connected to the power inverter, then the passive load is added to the inverter, and finally, a switching system is implanted to create different type of faults.

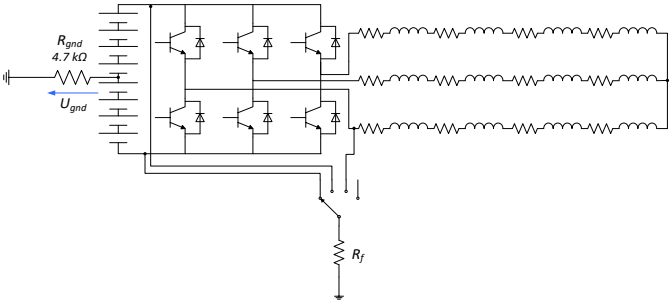

Fig. 20. Simplified electrical scheme of the experimental setup.

With the equipment installed, some tests were done. First, a healthy state was captured to ensure that the experiment runs correctly. After this, DC faults in the positive and negative poles of the batteries were done as well as AC faults. Now, some experimental results will be displayed.

B. *Healthy Condition tests*

Firstly, healthy condition tests were performed to ensure that the phase to neutral voltage waveforms in the AC side corresponds with the simulations. The results are displayed in Fig. 21.

The parasitic inductances and capacities induce sinusoidal filter effects in the voltage waveform, but the similarity with the simulations remains representative.

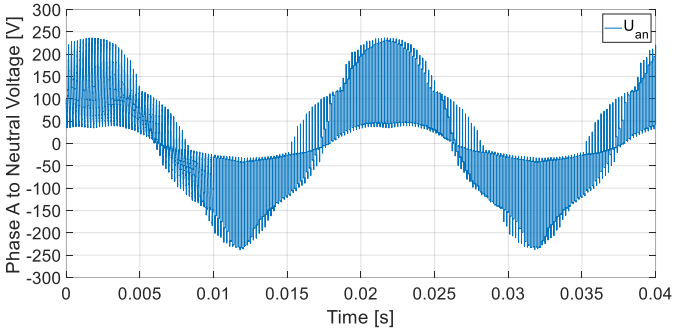

Fig. 21. Phase to neutral voltage for healthy operation conditions. (A Phase)

Then, the grounding resistor voltage measurement is performed. Fig. 22 shows how in the absence of a ground fault, the value obtained is zero. As in simulations, a high frequency fluctuation appears, but the average value remains null.

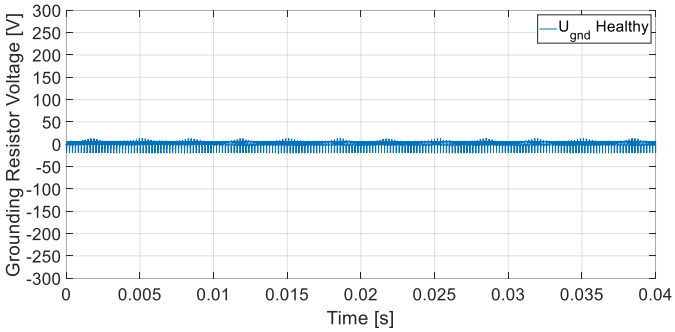

Fig. 22. Grounding resistor measurement for a healthy operation conditions.

C. *DC Side Positive pole ground fault tests*

Once the correct operation during the healthy state is corroborated, a huge number of ground faults have been carried out. First of all, some ground faults were done in the positive pole of the DC side obtaining the results shown in Fig. 23.

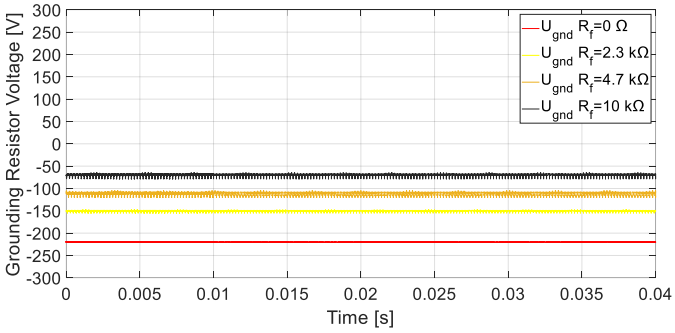

Fig. 23. Grounding Resistor Measurement for ground faults in positive pole of the DC side. [Fault resistances 0 Ω, 2.3 kΩ, 4.7 kΩ and 10 kΩ. R_{gnd} = 4.7 kΩ].

In the Fig. 23, the fault resistance was changed between the values of 0 Ω, 2.3 kΩ, 4.7 kΩ and 10 kΩ, obtaining constant voltage values where again the higher the resistance is, the lowest voltage is measured in the grounding resistor.

D. *DC Side Negative pole ground fault tests*

Then, faults in the negative pole with different ground fault resistances were made. The results are similar to those of the positive pole but with contrary sign, as can be seen in Fig. 24.

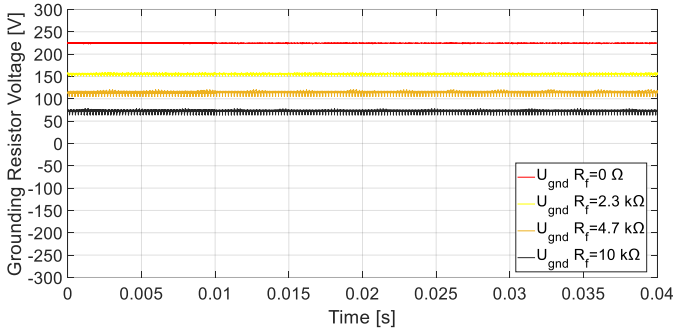

Fig. 24. Grounding Resistor Measurement for ground faults in negative pole of the DC side. [Fault resistances 0 Ω, 2.3 kΩ, 4.7 kΩ and 10 kΩ. R_{gnd} = 4.7 kΩ].

The sign of the voltage measurement is opposite to the pole where the fault occurs, i.e., a positive voltage measure implies a fault in the negative pole and a negative voltage measure implies a fault in the positive pole.

E. AC Side ground fault tests

Finally, AC faults were provoked in the power inverter terminals. The aim of these faults were to register an AC voltage waveform in terminals of the grounding resistor. The peak value of the wave would change with the ground fault resistance as in the cases before in a similar proportion, as expressed in (1). Furthermore, the AC phases from AC inverter terminals to neutral during a 2.3 kΩ ground fault in the phase A are plotted in Fig. 25. In this figure, no apparent difference can be appreciated among voltage waves with fault and healthy conditions (See Fig. 21).

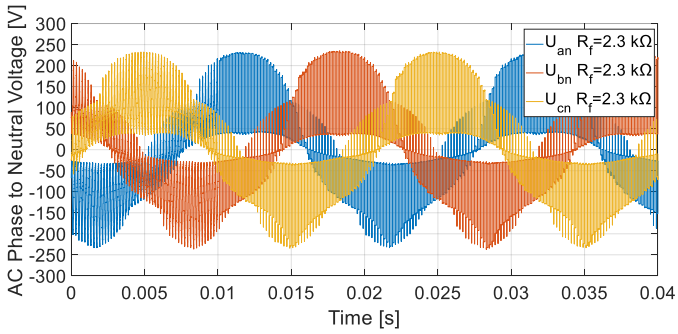

Fig. 25. Inverter AC voltages to neutral for 2.3 kΩ fault in phase A.

The grounding resistor voltage wave measurements are displayed in Fig. 26, Fig. 27, Fig. 28 and Fig. 29, for ground fault resistances of 0 Ω, 2.3 kΩ, 4.7 kΩ and 10 kΩ, respectively.

Also, the voltage wave in the grounding resistor is more sinusoidal when the inductance effects are higher. This is due to the direct relationship between voltage and leakage current circulating through ground by having only resistive part in the grounding device.

It can be observed some asymmetries in the voltage waveforms presented in this section, due to asymmetries in the manufacturing of the inverter, different parasitic capacitance to ground or difference reactance in phases. But they are not due to the use of grounding resistor.

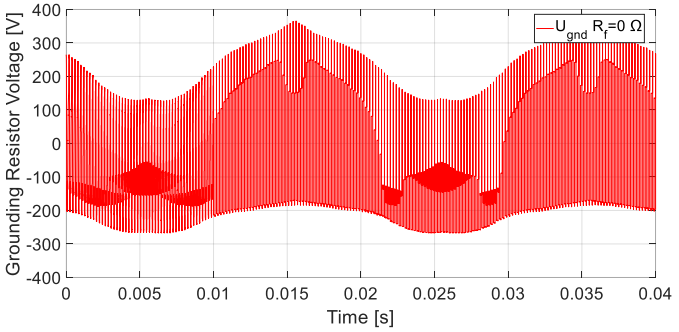

Fig. 26. Grounding resistor voltage waveform for a ground fault in the AC side. [Fault resistance 0 Ω. R_{gnd} = 4.7 kΩ].

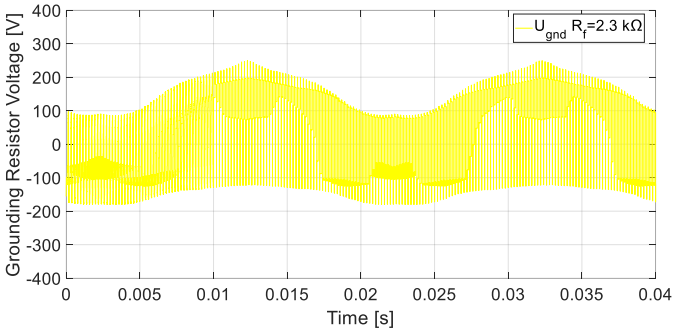

Fig. 27. Grounding resistor voltage waveform for a ground fault in the AC side. [Fault resistance 2.3 kΩ. R_{gnd} = 4.7 kΩ].

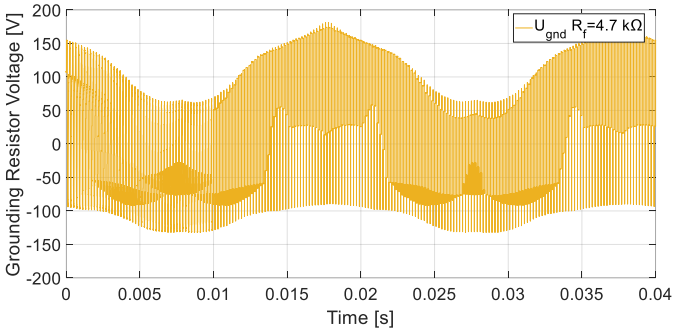

Fig. 28. Grounding resistor voltage waveform for a ground fault in the AC side. [Fault resistance 4.7 kΩ. R_{gnd} = 4.7 kΩ].

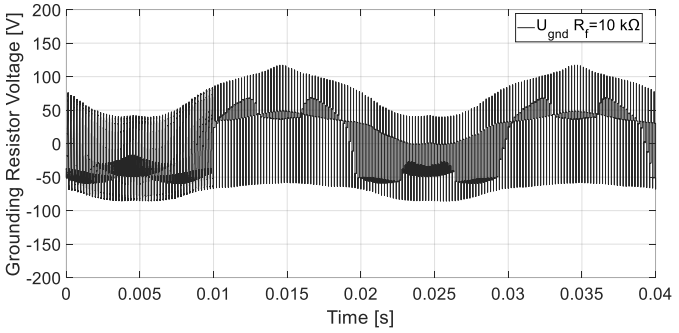

Fig. 29. Grounding resistor voltage waveform for a ground fault in the AC side. [Fault resistance 10 kΩ. R_{gnd} = 4.7 kΩ].

The grounding resistor voltage waves registered in the presented experimental tests have been analyzed by FFT. The results are collected in Table III. The fundamental inverter frequency (f_1 = 50Hz), the inverter commutation frequency (5 kHz) and the DC component are displayed.

As expected, it can be seen that for AC ground faults the fundamental inverter frequency component has remarkable

values in comparison with DC ground faults, where the DC components acquires higher importance.

TABLE III
GROUNDING RESISTOR VOLTAGE FFT EXPERIMENTAL RESULTS FOR DIFFERENT GROUND FAULTS

Type of fault and fault resistance, R_f	$\|U_{DC}\|$ [V]	$\|U_{f1}\|$ [V]	$\|U_{5kHz}\|$ [V]
DC Pole + ground fault			
$R_f = 0$	219.77	3.90×10^{-3}	0.01
$R_f = 2.3$ kΩ	150.69	5.22×10^{-3}	0.64
$R_f = 4.7$ kΩ	111.15	3.28×10^{-3}	1.62
$R_f = 10$ kΩ	70.25	9.53×10^{-3}	1.45
DC pole – ground fault			
$R_f = 0$	224.80	4.83×10^{-3}	7.09×10^{-3}
$R_f = 2.3$ kΩ	155.51	3.41×10^{-3}	0.67
$R_f = 4.7$ kΩ	113.89	7.39×10^{-3}	1.62
$R_f = 10$ kΩ	71.87	1.11×10^{-3}	1.44
AC phase ground fault			
$R_f = 0$	11.79	90.60	150.51
$R_f = 2.3$ kΩ	1.86	57.11	100.89
$R_f = 4.7$ kΩ	1.81	41.30	74.54
$R_f = 10$ kΩ	3.67	29.19	47.84

These satisfactory experimental results prove that it is possible to connect a grounding resistor between the midpoint of the batteries and the chassis, or ground, to ensure the detection and identification of ground faults in AC/DC systems.

To corroborate the theoretical principles, the experimental and simulation results are evaluated. The values of the grounding resistor voltage U_{gnd} are analyzed for different fault resistances R_f.

In order to compare the different ground faults, normalized values are employed. The voltage used to normalize U_{gnd} is $U_{DC}/2$, in case of DC ground fault, and $U_{an}(f_1)$, in case of AC fault. While the ground fault resistances are normalized dividing by R_{gnd} for any fault. Moreover, the theoretical grounding resistor voltage values, according to (1), are also plotted. The results are displayed in the Fig. 30.

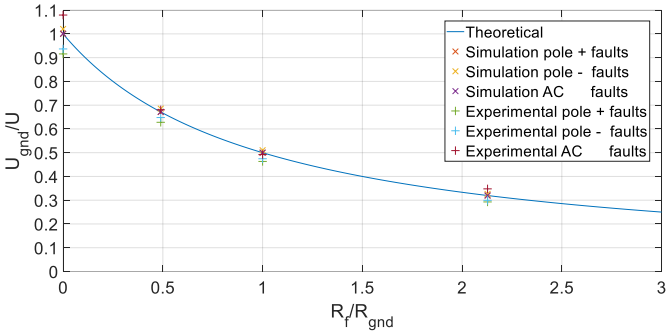

Fig. 30. Normalized grounding resistor voltage, U_{gnd}/U, versus normalized fault resistance, R_f/R_{gnd}, for different ground faults.

The obtained results verify the operation principle of this detection method.

VI. CONCLUSIONS

A new method for detection of ground faults in AC and DC sides of electric vehicles powertrain is presented in this paper.

It consists in measuring the voltage in terminals of a grounding resistor connected between the midpoint of the batteries and ground or chassis of the vehicle.

The detection is based on the analysis of the waveform of the grounding resistor voltage:

- If the waveform is zero, it implies a non-fault state.
- If the waveform is constant, the fault is in the DC bus, and depending on the polarity, it will be identified on the positive pole if the voltage is negative, and on the negative pole if the voltage is positive.
- If the waveform has an AC spectrum, a ground fault occurs in the AC side of the powertrain.

In order to prove these statements, numerous simulations and experimental tests have been carried out achieving good results.

The simulations results show that faults in the DC side are easily detected. The voltage amplitude measured depends on the fault resistance. Also, faults in the AC side can be perceived, measuring pulsed AC waves proportional to the leakage current. As in the DC case, the fault resistance affects the amplitude of the wave.

Moreover, the same phenomenon occurs in numerous experimental tests performed in a 140 kW power inverter. If a DC ground fault happens the voltage seen in the grounding resistor is constant. However, if the fault is in the AC side, the wave measured has a alternating profile.

The correspondence between simulations and experimental results corroborates this method and allows, with a ground resistor placed in the midpoint of the battery, to identify where the ground fault has occurred, hence saving maintenance and repair time.

ACKNOWLEDGMENT

The authors would like to thank Mrs. Allani, Mr. Lafoz and Mr. Gallo for their implication in this paper.

REFERENCES

[1] P. Tian, C. A. Platero, F. Blázquez and J. M. Guerrero, "Ground Fault Location System for Powertrain of Electric Vehicles," *2019 IEEE 12th International Symposium on Diagnostics for Electrical Machines, Power Electronics and Drives (SDEMPED)*, Toulouse, France, 2019, pp. 488-492.

[2] Yujie Wang, Jiaqiang Tian, Zonghai Chen, Xingtao Liu, "Model based insulation fault diagnosis for lithium-ion battery pack in electric vehicles," *Measurement*, Vol. 131, pp 443-451, 2019.

[3] D.L. Zhang, L.Y. Xiao, Y. Wang, G.Z. Huang, "Study on vehicle fire safety: Statistic, investigation methods and experimental analysis," *Safety Science*, Vol. 117, pp. 194-204, 2019.

[4] Asım Gökhan Yetgin, "Effects of induction motor end ring faults on motor performance. Experimental results," *Engineering Failure Analysis*, Vol. 96, pp. 374-383,2019,

[5] D. K. J. S. Jayamaha, N. W. A. Lidula and A. D. Rajapakse, "Ground Fault Analysis and Grounding Design Considerations in DC Microgrids," *2018 IEEE 4th Southern Power Electronics Conference (SPEC), Singapore*, Singapore, 2018, pp. 1-8.

[6] F. Candeletti, E. Tironi, M. Carminati and E. Ragaini, "LVDC microgrid with double ac grid interface: Protection against dc ground faults and control strategies," *2018 18th International Conference on Harmonics and Quality of Power (ICHQP)*, Ljubljana, 2018, pp. 1-8.

[7] X. Han, W. Sima, M. Yang, L. Li, T. Yuan and Y. Si, "Transient Characteristics Under Ground and Short-Circuit Faults in a ±500 kV MMC-Based HVDC System With Hybrid DC Circuit Breakers," *in IEEE Transactions on Power Delivery, vol. 33, no. 3, pp. 1378-1387*

[8] J. Park, "Ground Fault Detection and Location for Ungrounded DC Traction Power Systems," *in IEEE Transactions on Vehicular Technology*, vol. 64, no. 12, pp. 5667-5676, Dec. 2015.

[9] Y. Wang, Z. Yu, J. He, S. Chen, R. Zeng and B. Zhang, "Performance of Shipboard Medium-Voltage DC System of Various Grounding Modes Under Monopole Ground Fault," *in IEEE Transactions on Industry Applications*, vol. 51, no. 6, pp. 5002-5009, Nov.-Dec. 2015.

[10] A. Dimitriou and C. A. Charalambous, "DC Interference Modeling for Assessing the Impact of Sustained DC Ground Faults of Photovoltaic Systems on Third-Party Infrastructure," in *IEEE Transactions on Industrial Electronics*, vol. 66, no. 4, pp. 2935-2945, April 2019.

[11] A. Ulatowski and A. M. Bazzi, "A Combinational-Logic Method for Electric Vehicle Drivetrain Fault Diagnosis," *in IEEE Transactions on Industry Applications*, vol. 52, no. 2, pp. 1796-1807, March-April 2016.

[12] L. Zhang, Y. Fan, R. D. Lorenz, R. Cui, C. Li and M. Cheng, "Design and Analysis of a New Five-Phase Brushless Hybrid-Excitation Fault-Tolerant Motor for Electric Vehicles," *in IEEE Transactions on Industry Applications*, vol. 53, no. 4, pp. 3428-3437, July-Aug. 2017.

[13] L. Wei and Z. Liu, "Identifying ground fault location in High Resistance Grounded systems for Adjustable Speed Drive at low speed," *2012 IEEE Energy Conversion Congress and Exposition (ECCE)*, Raleigh, NC, 2012, pp. 3609-3616.

[14] H. F. Habib, M. M. Esfahani and O. A. Mohammed, "Investigation of Protection Strategy for Microgrid System Using Lithium-Ion Battery During Islanding," in *IEEE Transactions on Industry Applications*, vol. 55, no. 4, pp. 3411-3420, July-Aug. 2019.

[15] Yujie Wang, Jiaqiang Tian, Zonghai Chen, Xingtao Liu, "Model based insulation fault diagnosis for lithium-ion battery pack in electric vehicles," *Measurement*, Volume 131, 2019, pp 443-451.

[16] J. A. Marrero, "Understand ground fault detection and isolation in DC systems," *2000 Power Engineering Society Summer Meeting (Cat. No.00CH37134)*, Seattle, WA, 2000, pp. 1707-1711 vol. 3.

[17] H. Duffy, J. Chiang, J. Midgley and B. Thomas, "Circuit protection arrangements using ground fault interrupter for overcurrent and overvoltage protection," U.S. Patent 563 321, Nov. 28, 1995.

[18] Z. Noworolski and U. Reskov, "Ground Fault Detection by Differential Monitoring of the Float Current," *INTELEC 06 - Twenty-Eighth International Telecommunications Energy Conference*, Providence, RI, 2006, pp. 1-5.

[19] M. Yano and T. Takeshita, "Electric vehicle with ground fault detecting system," U.S. Patent, No 8164344B2. Apr. 24, 2012.

[20] Yang and T. Okada, "Apparatus for detecting leakage current of battery," U.S. Patent, No 2012/0229142A1, Sep. 13, 2012.

[21] F. Saidani, F.X. Hutter, W. Selinger, S. Rößler, W. Braunwarth, J.N. Burghartz, "An integrated electronic circuit for decentralized monitoring of Lithium-ion battery cells", *MikroSystem Technik Kongress*, 2017, pp. 566-569, 2017.

[22] Granizo, R.; Blánquez, F.; Rebollo, E.; Platero, C. "A Novel Ground Fault Non-Directional Selective Protection Method for Ungrounded Distribution Networks," *Energies* , 2015, 8(2), pp. 1291-1316.

[23] S. Wen, et al. "Relay protection distance setting value check method based on measured impedance," CN Patent No 106385014A, Feb. 8, 2017.

[24] C. A. P. Gaona, F. Blázquez, P. Frías and M. Redondo, "A Novel Rotor Ground-Fault-Detection Technique for Synchronous Machines With Static Excitation," *in IEEE Transactions on Energy Conversion*, vol. 25, no. 4, pp. 965-973, Dec. 2010.

[25] C. A. Platero, F. Blázquez, P. Frías and M. Pardo, "New On-Line Rotor Ground Fault Location Method for Synchronous Machines with Static Excitation," *in IEEE Transactions on Energy Conversion*, vol. 26, no. 2, pp. 572-580, June 2011.

AUTHORS' INFORMATION

José Manuel Guerrero was born in 1996 in Madrid, Spain. He obtained his Bachelor degree in Energy Resources, Fuels and Explosive Engineering from the Universidad Politécnica of Madrid, Spain, in 2018. He received his Master degree in Electrical Engineering from Universidad Politécnica de Madrid (Spain) in 2019.

He worked as researcher in Laboratorio Oficial Madariaga S.L. in 2018 in alternative tests for electrical machines parameters characterization. He is currently working on measuring device calibration procedures in the Department of Energy and Fuels at the Universidad Politécnica of Madrid.

Gustavo Navarro was born in 1982 in Madrid, Spain. He received his degree in electronic engineering from the Universidad Politécnica de Madrid, Spain, in 2007.

Since 2007 he has been working as a research engineer in the Electrical Engineering Group at CIEMAT (Spanish Public Research Centre on Energy, Environment and Technology). His topics of interest are electrical drives control, energy storage systems (batteries and supercapacitors) and power electronics hardware design and validation.

Carlos A. Platero (M´10) was born in Madrid, Spain, in 1972. He obtained his Dipl. degree and Ph.D. degree in Electrical Engineering from the Universidad Politécnica de Madrid, Spain, in 1996 and 2007 respectively.

From 1996 to 2008 he worked in ABB Generación S.A., Alstom Power S.A. and ENDESA Generación SA, and was involved in the design and commissioning of power plants.

In 2002 he started teaching at the Electrical Engineering Department of the Universidad Politécnica de Madrid, and joined an energy research group. In 2008 he became a full-time Associate Professor.

Pengfei Tian was born in Xi'an, Shaanxi, China, in 1991. He received his Bachelor degree in Electrical Engineering from Shaanxi Science and Technology University (China) in 2014. He received his Master degree in Electrical Engineering from Universidad Politécnica de Madrid (Spain) in 2018.

Francisco Blázquez (M´09) was born in Toledo, Spain, in 1972. He received the Dipl. degree in Industrial Engineering and the Ph.D. degree in Electrical Engineering from the Universidad Politécnica de Madrid, Spain in 1997 and 2004, respectively.

The Since 1999 he has been professor at the Electrical Engineering Department at the Universidad Politécnica de Madrid.

His current research interests include electrical machine design and wind power generation.